Rakenteiden Mekaniikka (Journal of Structural Mechanics) Vol. 58, No. 4, 2025, pp. 174–185 http://rakenteidenmekaniikka.journal.fi https://doi.org/10.23998/rm.152545 © 2025 The Authors

Open access under the license CC BY 4.0



# Phase field method for brittle fracture implemented with polygonal finite elements

Timo Saksala<sup>1</sup>, Mahmood Jabareen and Reijo Kouhia

**Summary** The aim of this article is to model fracture propagation in brittle materials, such as rocks and concrete, with the phase field approach. The hybrid formulation of the phase field theory is adopted because it enables using an ad-hoc, or a problem specific, crack driving force, here of Mohr–Coulomb type, to correctly model brittle materials under compression or shear. Hybrid formulations are variationally inconsistent because the crack driving force is not the same as the one used in the underlying energy functional. They are, however, thermodynamically consistent, and computationally cheap since they allow to use a linear balance of momentum equation within the robust staggered scheme to solve the coupled system for the phase field and the displacement field. The phase field method is implemented with 2D polygonal finite elements based on the Wachspress interpolation functions. As numerical examples, typical test cases of notched samples under mode I and II loadings are simulated. Finally, a slope stability problem is solved as an engineering application.

Keywords: phase field method, hybrid formulation, polygonal finite elements, brittle fracture

Received: 2 December 2024. Accepted: 15 July 2025. Published online: 27 October 2025.

#### Introduction

Phase field method has become an extremely popular approach to model fracture in computational mechanics during the last two decades, see e.g. [1–12]. Its attraction stems from the ability to simulate crack initiation, propagation, and branching without the need for ad-hoc criteria. Moreover, with this method, cracks are tracked automatically by the propagation of a smooth crack field on a fixed mesh. However, the major shortcoming is the computational labour due to dense meshes required to reach reasonable accuracy. In addition, it is challenging to find a suitable crack, or phase field, driving force for compressive/shear fractures, especially for brittle materials under uniaxial compression

<sup>&</sup>lt;sup>1</sup> Corresponding author: timo.saksala@tuni.fi

[7,8]. An ad-hoc choice of a crack driving force and its split into volumetric and deviatoric components (in order to separate model behavior in compression and tension) suitable for modelling shear banding in geomaterials leads to a hybrid formulation, which is variationally inconsistent. Variational inconsistency here means that the crack driving force is not the same as the one used in the underlying energy functional from which the expressions for the stress and the elasticity tensor are derived [11,12]. However, these formulations are usually thermodynamically consistent [11,12]. For a review on the historical developments of the method, see [12].

Polygonal finite elements have also attracted considerable attention in computational mechanics during last couple of decades [13–16]. Compared to traditional triangular and rectangular elements (in 2D), the perform better in meshing arbitrary geometries, describe better the grain texture of some materials (e.g. rocks), and have less locking-prone behavior under volume-preserving deformation [13]. However, the main drawback is the much more involved numerical integration [14] because the interpolation functions are, e.g., rational functions [17].

In the present work, we implement the phase field method with polygonal finite elements based on the Wachspress interpolation functions [17]. The aim is to model fracture propagation in brittle materials, such as rocks and concrete. For this reason, the hybrid formulation of the phase field theory is adopted. Moreover, this formulation is computationally cheap since it allows to use a linear balance of momentum equation within the robust staggered scheme to solve the coupled system for the phase field and the displacement field. The novelty of the present model is in the judicious combination of the polygonal finite elements and the phase field fracture model for brittle materials with a Mohr–Coulomb and Rankine criteria type of fracture driving forces. There is a previous paper by Li and Cui [18] combining the polygonal finite elements and the phase field model for fracture, but it is based on the typical positive-negative parts split of the strain tensor and is thus not suitable for shear failure in brittle materials. As numerical examples, typical benchmark problems of notched samples under mode I and II loadings are solved. Finally, a slope stability problem is solved as an engineering application.

#### Phase field model for brittle fracture

#### Standard variationally consistent formulation

In the phase field method for fracture, an internal discontinuity  $\Gamma_{\phi}$  in an elastic body  $\Omega$  (see Figure 1) is represented by a smooth phase field variable  $\phi$  over a finite width  $l_c$ , called a length scale. The phase field variable, akin to the damage variable, ranges from 0, for an intact material, to 1 for a fully cracked material. The governing equations of this problem are derived by a variational approach [4,11]. Consider the regularized energy functional for the fractured body originally presented by Bourdin et al. [18]:

$$L = \int_{\Omega} \psi_{\varepsilon}(\mathbf{\varepsilon}, \phi) d\Omega + \int_{\Omega} G_{c} \gamma(\phi, \nabla \phi) d\Omega - \int_{\Omega} \mathbf{b} \cdot \mathbf{u} d\Omega - \int_{\partial \Omega_{c}} \mathbf{t} \cdot \mathbf{u} dS$$
 (1)

$$\psi_{\varepsilon}(\mathbf{\varepsilon}, \phi) = g(\phi)\psi_{0}(\mathbf{\varepsilon}) = ((1 - \phi)^{2} + k)(\frac{\lambda}{2} \operatorname{tr}(\mathbf{\varepsilon})^{2} + \mu \operatorname{tr}(\mathbf{\varepsilon}^{2}))$$
 (2)

where  $\varepsilon$  is the strain tensor,  $\psi_0$  is the elastic strain energy defined with the Lame constants  $\lambda$ ,  $\mu$ . Moreover,  $G_c$  is the critical energy release rate, **b** is a body force (gravity here), **t** is the prescribed traction,  $\mathbf{u}$  is the displacement vector, and k is a small numerical parameter to avoid singularities upon solving the equations. Furthermore,  $g(\phi)$  is the typically applied quadratic degradation function. Finally, the regularization term, i.e., the crack surface density function, reads

$$\gamma(\phi, \nabla \phi) = \frac{1}{2l_c} \phi^2 + \frac{l_c}{2} |\nabla \phi|^2. \tag{3}$$

The governing equations can now be derived with the standard steps requiring that the first variation of the functional L disappears, i.e.,  $\delta L = 0$ , which leads following system of model equations:

$$\nabla \cdot \mathbf{\sigma} + \mathbf{b} = \mathbf{0} \tag{4}$$

$$G_c l_c \nabla^2 \phi - \frac{G_c}{l_c} \phi + 2(1 - \phi) H_p = 0 \tag{5}$$

$$\mathbf{\sigma} = g(\phi) \frac{\partial \psi_0}{\partial \mathbf{s}} = ((1 - \phi)^2 + k) [\lambda \operatorname{tr}(\mathbf{s})\mathbf{I} + 2\mu \mathbf{s}]$$
 (6)

$$G_{c}l_{c}\nabla^{2}\phi - \frac{G_{c}}{l_{c}}\phi + 2(1 - \phi)H_{p} = 0$$

$$\sigma = g(\phi)\frac{\partial\psi_{0}}{\partial\varepsilon} = ((1 - \phi)^{2} + k)[\lambda tr(\varepsilon)\mathbf{I} + 2\mu\varepsilon]$$

$$\mathbf{D}_{e\phi} = g(\phi)\frac{\partial^{2}\psi_{0}}{\partial\varepsilon^{2}} = ((1 - \phi)^{2} + k)\mathbf{D}_{e}$$
(6)
$$(7)$$

where the symbol meaning are:  $\mathbf{D}_e$  is the standard elasticity tensor;  $\mathbf{I}$  is the second order unit tensor and  $H_p = \max(\psi_0)$  is the maximum positive strain energy during the strain history, and it prevents healing of the crack. Equation (6) defines the stress tensor, while Equation (4) is the standard balance of linear momentum, and Equation (5) governs the evolution of the phased field damage  $\phi$ . In order to solve this system, boundary conditions need to be specified:  $\mathbf{\sigma} \cdot \mathbf{n} = \overline{\mathbf{t}}$  and  $\mathbf{u} = \overline{\mathbf{u}}$  on relevant parts of the boundary (see Figure 1) and  $\nabla \phi \cdot \mathbf{n} = 0$  on  $\Gamma_{\phi}$ . This is the standard variationally consistent formulation for linear elastic isotropic solids with isotropic stress degradation.

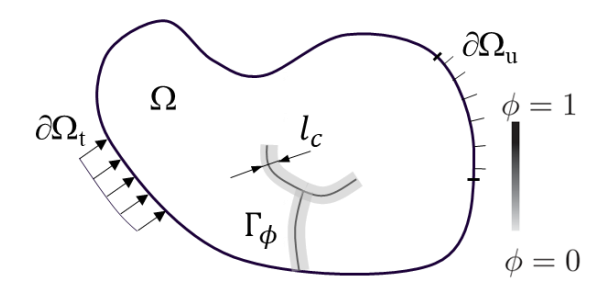


Figure 1. Schematic illustration of a body with a crack represented by a smooth phase field with a finite width.

#### Present hybrid formulation

The crack driving force in the standard formulation above is the isotropic elastic energy, which cannot predict correct failure modes in shear dominated applications. For this reason, hybrid formulations have been proposed where ad-hoc crack driving forces are chosen for specific applications and materials, as discussed in Introduction above. The

present formulation is inspired by Refs. [7] and [11]. In the previous study by Zhou et al., a Mohr–Coulomb type of crack driving force is employed in modelling shear fracture in rock-like materials. The latter work by Zhang et al., likewise on rock-like materials, splits the crack driving force into two components,  $H = H_I + H_{II}$ , where the components are based on the volumetric and deviatoric split of the elastic energy. The present hybrid formulation similarly employs the concept of splitting the crack driving force into separate components for tensile and compressive failures. However, instead of positive-negative or volumetric-deviatoric parts decompositions, the Rankine and Mohr–Coulomb criteria type of crack driving forces are chosen. This requires a modification of the phase field evolution equation so that the model now becomes:

$$l_c \nabla^2 \phi - \frac{1}{l_c} \phi + 2(1 - \phi) \left( \frac{H_t}{G_{Ic}} + \frac{H_s}{G_{IIc}} \right) = 0$$
 (8)

$$H_t = \max_{\tau \in [0,t]} \frac{1}{2E} \left\langle \sqrt{\langle \sigma_1 \rangle_+^2 + \langle \sigma_2 \rangle_+^2} - \sigma_t \right\rangle_+^2 \tag{9}$$

$$H_{s} = \max_{\tau \in [0,t]} \frac{1}{2\mu} \langle \langle -\sigma_{1} \rangle - \langle -\sigma_{3} \rangle + (\langle -\sigma_{1} \rangle + \langle -\sigma_{3} \rangle) \sin(\varphi) - 2c_{0} \cos(\varphi) \rangle^{2}$$
 (10)

where  $\sigma_i$  is the *i*th principal stress,  $G_{Ic}$  and  $G_{IIc}$  are mode I and II fracture energies,  $\sigma_t$  is the tensile strength, and  $\varphi$  and  $c_0$  are the internal friction and the cohesion of the material. Moreover, Macaulay brackets (the positive part operator) have been used. It can be observed that the expression in Equation (9) inside the Macaulay brackets is the rounded Rankine criterion while the one in Equation (9) is the Mohr–Coulomb criterion.

Due to the stress-based crack driving forces (9) and (10), the mechanical part is kept unaltered so that Equation (6) and (7) are still valid. This means that the present approach is isotropic in that the elastic energy is not split, e.g., into volumetric and deviatoric components (see [7] for more info).

### Finite element form of the equations and their solution

The finite elements versions of the Equation (4) and (5) are derived by standard steps using the principle of virtual work. Following Miehe et al. [4] and Navidtehrani et al. [6], the governing equations are solved with the staggered scheme. Applying the Newton–Raphson method for the subsystems, the resulting equations for solving the displacement  $\bf u$  and phase field  $\bf \phi$  are written as:

$$\begin{bmatrix} \mathbf{K}_{u}^{n} & \mathbf{0} \\ \mathbf{0} & \mathbf{K}_{\phi}^{n} \end{bmatrix} \begin{pmatrix} \mathbf{u}_{n+1} \\ \mathbf{\phi}_{n+1} \end{pmatrix} = - \begin{pmatrix} \mathbf{R}_{u}^{n} \\ \mathbf{R}_{\phi}^{n} \end{pmatrix}$$
(11)

where

$$\mathbf{K}_{u} = \mathbf{A}_{e=1}^{N_{e}} \int_{\Omega} ((1 - \phi)^{2} + k) \, \mathbf{B}_{ue}^{T} \mathbf{D}_{e} \mathbf{B}_{ue} d\Omega$$
 (12)

$$\mathbf{R}_{u} = \mathbf{A}_{e=1}^{N_{e}} \left( \int_{\Omega} \left( (1 - \phi)^{2} + k \right) \mathbf{B}_{ue}^{T} \mathbf{\sigma} \, d\Omega - \int_{\Omega} \mathbf{N}_{ue}^{T} \mathbf{b} \, d\Omega - \int_{\partial \Omega_{r}} \mathbf{N}_{ue}^{T} \mathbf{t} \, dS \right)$$
(13)

$$\mathbf{K}_{\phi} = \mathbf{A}_{e=1}^{N_e} \int_{\Omega} \left( l_c \mathbf{B}_{\phi e}^T \mathbf{B}_{\phi e} + \left( \frac{1}{l_c} + \frac{2H_c}{G_{IC}} + \frac{2H_s}{G_{IC}} \right) \mathbf{N}_{\phi e}^T \mathbf{N}_{\phi e} \right) d\Omega$$
(14)

$$\mathbf{R}_{\phi} = \mathbf{A}_{e=1}^{N_e} \left( \int_{\Omega} \left( \frac{1}{l_c} \phi - 2(1 - \phi) \left( \frac{H_t}{G_{Ic}} + \frac{H_s}{G_{IIc}} \right) \right) \mathbf{N}_{\phi e}^T + l_c \mathbf{B}_{\phi e}^T \nabla \phi \right) d\Omega$$
 (15)

The notations here are:  $\mathbf{K}_u$  and  $\mathbf{K}_{\phi}$  are the stiffness matrices for displacement and phase field equations, respectively;  $\mathbf{R}_u$  and  $\mathbf{R}_{\phi}$  are the residual vectors for displacement and phase field equations, respectively;  $\mathbf{A}$  is the standard finite element assembly operator;  $\mathbf{B}_{ue}$  and  $\mathbf{B}_{\phi e}$  are the gradient operators for displacement and phase field ( $\mathbf{\varepsilon} = \mathbf{B}_{ue}\mathbf{u}_e, \nabla \phi = \mathbf{B}_{\phi e}\mathbf{\phi}$ ), respectively;  $\mathbf{N}_{ue}$  and  $\mathbf{N}_{\phi e}$  are the interpolation matrices for displacement and phase field variables, respectively. The interpolation mappings are standard, i.e.,  $\mathbf{u} = \mathbf{N}_{ue}\mathbf{u}_e$ ,  $\phi = \mathbf{N}_{\phi e}\mathbf{\phi}_e$  with  $\mathbf{u}_e$  and  $\mathbf{\phi}_e$  being the nodal displacement and phase field vectors, respectively, for element e. It should be noted that the solution of Equation (11) is fast and robust due to the isotropic form of the stiffness matrix (12).

# Polygonal element based on Wachspress interpolation

The implementation of Talischi et al. [16] of the polygonal finite element method based on Wachspress interpolation functions is chosen. It exploits the standard isoparametric mapping from a reference element to the physical element, as illustrated in Figure 2. Mathematically, a Wachspress type of barycentric interpolant at node i of a reference n-gon reads

$$N_{i}(\xi) = \frac{\alpha_{i}(\xi)}{\sum_{j=1}^{n} \alpha_{j}(\xi)}, \quad \alpha_{i}(\xi) = \frac{A(p_{i-1}, p_{i}, p_{i+1})}{A(p_{i-1}, p_{i}, \xi)A(p_{i}, p_{i+1}, \xi)}$$
(16)

where A(a, b, c) denotes the signed area of triangle a, b, c (Figure 2a). The numerical integration is carried out by sub-dividing the reference polygon into triangles and using a three-point Hammer integration scheme for each triangle (resulting 3n integration points for each n-gon), as illustrated in Figure 2b.

The polygonal element mesh is generated by the open source PolyMesher Matlab code by Talischi et al. [15]. This code generates 2D Voronoi diagrams (tessellations) consisting of centroidal (or alternatively non-centroidal) Voronoi cells.

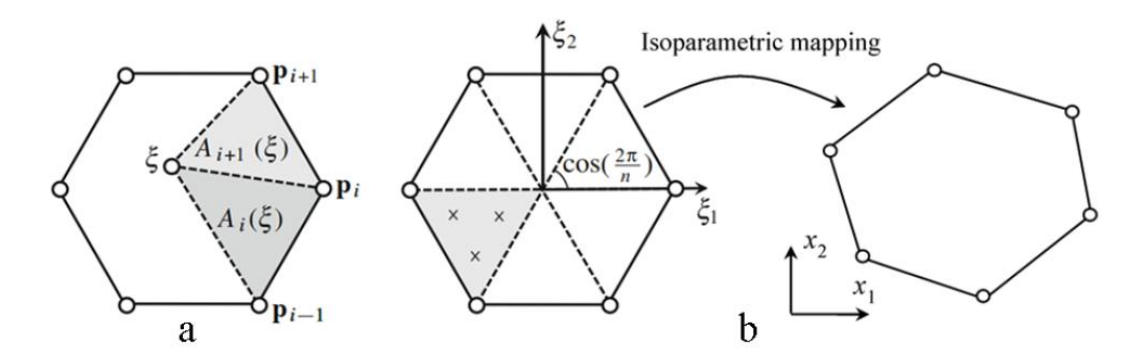


Figure 2. Polygonal element: Triangular areas used in the definition of Wachspress shape function (a); Triangulation of the reference regular polygon with three integration points in each triangle, and the isoparametric mapping to a physical element (b).

### **Numerical examples**

A representative set of typical benchmark problems are solved here with the present phase field formulation. Moreover, a mesh sensitivity study, guiding the mesh design in each problem, is performed in Appendix A. All simulations are performed with a self-written Matlab code.

# Single edge notched tests

This test is a benchmark case used extensively in the phase field for fracture literature. The geometry and the boundary conditions for the two cases tested here are shown in Figure 3a. The computations are carried out by controlling the displacement vertically in LC1 and horizontally in LC2. In the latter case, the vertical displacement of the nodes in the mesh (shown in Figure 3b) is also restricted. The material properties and model parameters are as follows: E = 210 GPa; v = 0.3;  $\sigma_t = 2445.42 \text{ MPa}$ ;  $G_{Ic} = 2700 \text{ J/m}^2$ ;  $I_c = 0.0075 \text{ mm}$ .

The predicted crack path in LC1, shown in Figure 3c, is as expected, i.e., the crack initiates at the tip of the pre-notch and propagates straight through the sample horizontally. In LC2, the crack propagates downwards with a curvy trajectory and, due to the shear nature of the loading and the restricted vertical degrees of freedom, reaches the bottom edge first and then the right vertical edge. In both cases the predicted cracks agree to those found in the literature, see e.g. [9].

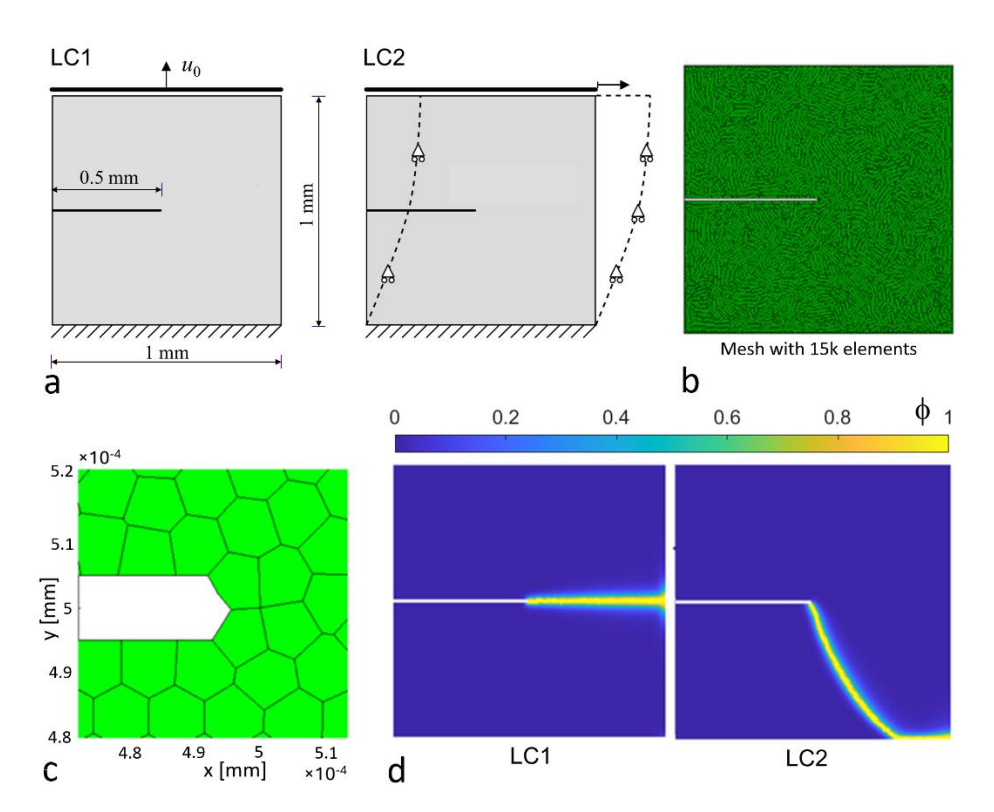


Figure 3. Simulation results for single edge notched tests: Test geometry and load cases (a); Polygonal finite element mesh with 15000 polygons (b); A magnified detail at the edge of the pre-notch (c); the predicted crack patterns in terms of the phase field variable (d).

# Mixed mode I or mode II crack propagation in a pre-notched PMMA specimen

This test is used, e.g., by Pham et al. [10] to validate their phase-field model. The PMMA specimen (dimensions in mm) is shown in Figure 4a. In the experimental setting, a sharp crack, of 13.47 mm long in the present case, is created by impacting a razor blade against the tip of 4 mm wide and 22.86 mm long pre-notch. The specimen is similar to the standard compact test specimen except the extra hole (10 mm of diameter), which disrupts the symmetric stress field so that the crack path proceeds curvilinearly, reaching the extra hole as illustrated in Figure 4a (the red dotted line after [10]). Loading is imposed at constant velocity at points A and B at rate 4E-4 mm/s. The thickness of the sample is 3 mm. The material properties and model parameters are: E = 2.98 GPa; v = 0.35;  $\sigma_t = 50$ MPa;  $G_{Ic} = 285 \text{ J/m}^2$ ;  $l_c = 0.5\text{E}-3 \text{ m}$ . The polygonal mesh with only 5000 elements is shown in Figure 4b. The relatively economic mesh is due to a refinement (requires modifications to the PolyMesher code) around the expected crack path. Moreover, the sharp pre-crack is here modelled as a topological entity with a width of 0.33 mm. The element size at the crack tips is about 0.27 mm. Alternatively, it could be modelled as a boundary condition for the phase field, i.e., the phase field variable having value 1 at the mesh nodes on both sides of the crack. However, this method also requires tailoring the mesh details [10]. The predicted crack path agrees with the experimental one quite well, as observed in Figure 4d.

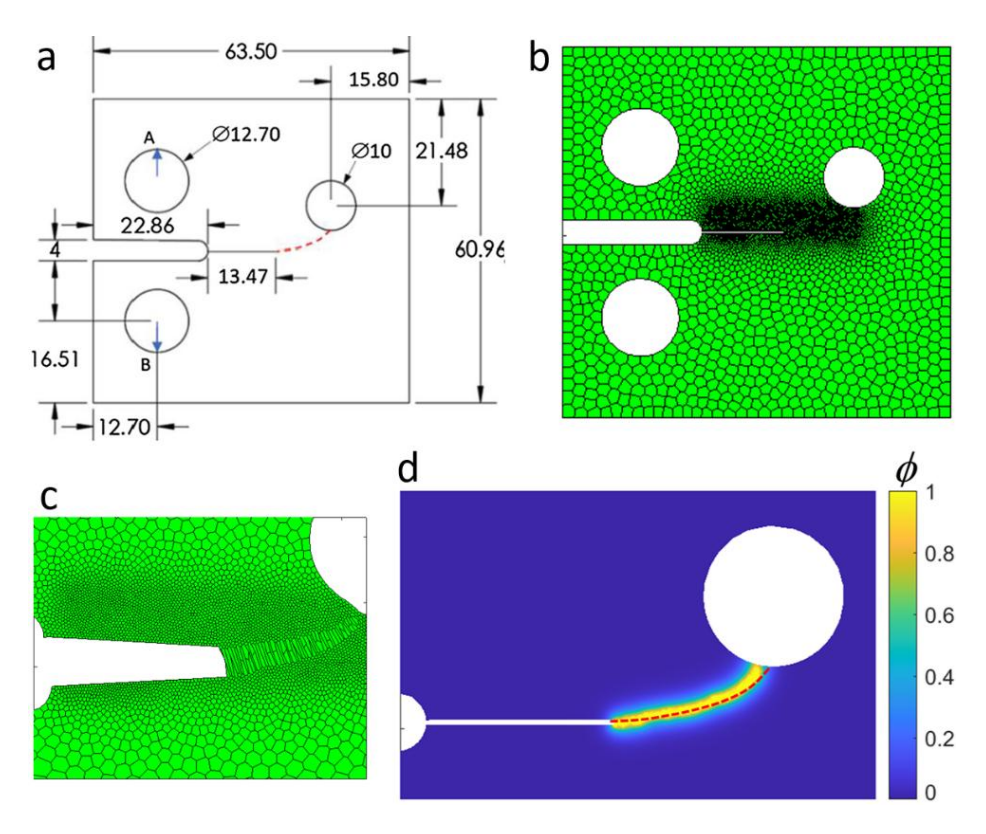


Figure 4. Simulation results for the pre-notched PMMA specimen: Test geometry and load cases (a); Polygonal finite element mesh with 5000 polygons (b); Deformed mesh with magnification (c); the predicted crack pattern compared to the experimental one (after [10]) (d).

# Engineering problem: Slope stability under self-weight

A geotechnical engineering problem of slope stability under self-weight is solved as the final numerical example. More specifically, the problem concerns a homogenous 2D soil slope with critical dimensions so that instability occurs with the unit weight  $\gamma = 20 \text{ kN/m}^3$ , cohesion  $c_0 = 12.38 \text{ kPa}$  and the friction angle  $\varphi = 20^\circ$ . The Young's modulus and Poisson's ratio are 10 MPa and 0.4, respectively. The phase field model parameters are:  $G_{IIc} = 200 \text{ N/m}$  and  $l_c = 0.15 \text{ m}$ . The polygonal element mesh with 15000 elements and the boundary conditions are shown in Figure 5a. The element size is  $\approx 100 \text{ mm}$ . The loading is applied gradually so that  $\gamma = 20 \text{ kN/m}^3 \cdot n/100 \text{ for } n < 100$ , and  $\gamma = 20 \text{ kN/m}^3 \cdot n/100 \text{ for } n < 100$ . The red dashed line in Figure 5a sketches the theoretical and experimental toe failure mode.

The predicted failure type is the toe failure, i.e., the instability failure initiates at the toe of the slope and propagates towards to the top of the slope. However, the failure band does not reach the top edge of the slope but deviates towards the right edge of the meshed domain, as can be observed in Figure 5c. Nevertheless, this prediction agrees with that by Wang et al. [8] using also the phase field approach. It is important to emphasize that this is not a problem related to the Mohr–Coulomb criterion because it can predict the correct failure band (reaching the top edge) when used as a yield criterion in a plasticity model, as demonstrated by Xiang & Zi-Hang [19]. The problem thus seems to be in the present phase field formulation itself.

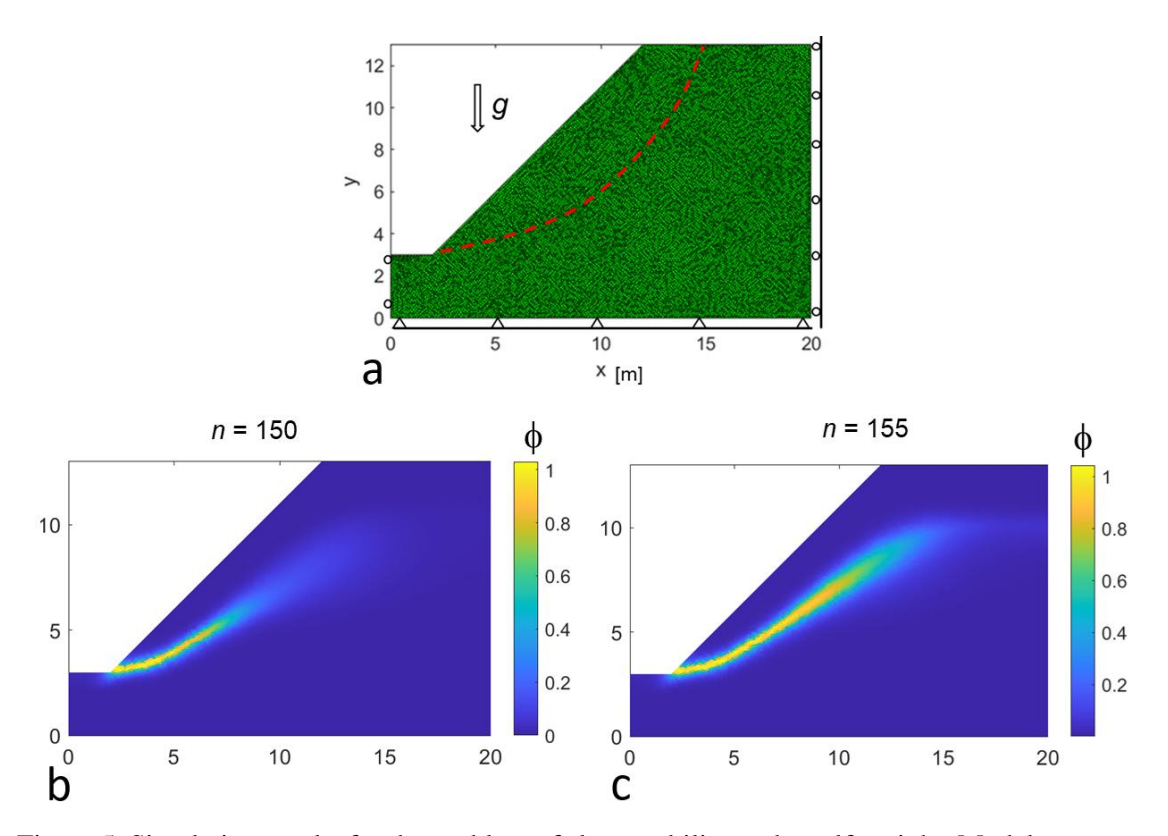


Figure 5. Simulation results for the problem of slope stability under self-weight: Model geometry and the boundary conditions shown with the polygonal mesh (15000 polygons) (a); the predicted failure mode at loading step n = 150 (b) and at n = 150 (c).

#### **Conclusions**

A phase field model for brittle fracture was implemented with polygonal finite elements based on the Wachspress rational interpolants. The phase field model was formulated as a hybrid, i.e., the elastic energy used in the variational formulation does not drive the fracture (the phase field evolution). Instead, the fracture is driven by separate, stress-based crack driving forces, of the Rankine and Mohr–Coulomb type, respectively, for tensile and compressive failures. However, the elastic energy is employed, in its isotropic form, to calculate stress and material stiffness (elasticity tensor). Within the staggered solution strategy for the coupled system, it follows from this feature that the tangent stiffness operator remains linear and therefore its solution is fast and robust.

The main drawback of the present hybrid-isotropic formulation is that it ignores the unilateral effects of damage in tension and compression and is thus not suitable for cyclic loadings. Moreover, the polygonal elements are computationally more intensive than the traditional finite elements due to the rational interpolants. The present combination was also found to be somewhat mesh sensitive. Nevertheless, the present method was successfully applied to some benchmark problems in the phase field literature, and it performed very well. However, the phase field method, at least the present formulation, fails partially to predict the correct failure mode in a slope stability problem under self-weight. The method predicts the correct failure initiation at the toe of the slope, but it does not reach the top of the slope. This issue should be studied more in future. Finally, a study comparing the performance of the traditional finite elements and the polygonal ones in modelling crack propagation in brittle materials with the phase field approach is needed.

#### References

- [1] B. Bourdin, G.A. Francfort, J.J. Marigo. The Variational Approach to Fracture. *Journal of Elasticity*, 91: 5–148, 2008. https://doi.org/10.1007/s10659-007-9107-3
- [2] A. Mesgarnejad, B. Bourdin, M.M. Khonsari. Validation simulations for the variational approach to fracture. *Computer Methods in Applied Mechanics and Engineering*, 290:420–437, 2015. https://doi.org/10.1016/j.cma.2014.10.052
- [3] A. Emdadi, M. Asle Zaeem. Phase-field modeling of crack propagation in polycrystalline materials. *Computational Materials Science*, 186, 110057, 2021, https://doi.org/10.1016/j.commatsci.2020.110057
- [4] C. Miehe, M. Hofacker, F. Welschinger. A phase field model for rate-independent crack propagation: Robust algorithmic implementation based on operator splits. *Computer Methods in Applied Mechanics and Engineering*, 199: 2765–2778, 2010. https://doi.org/10.1016/j.cma.2010.04.011
- [5] A. Pandolfi, K. Weinberg, M. Ortiz. A comparative accuracy and convergence study of eigenerosion and phase-field models of fracture. *Computer Methods in Applied Mechanics and Engineering*, 386, 114078, 2021. https://doi.org/10.1016/j.cma.2021.114078
- [6] Y. Navidtehrani, C. Betegón, E. Martínez-Pañeda. A simple and robust Abaqus implementation of the phase field fracture method. *Applications in Engineering Science*, 6, 100050, 2021. https://doi.org/10.1016/j.apples.2021.100050

- [7] S. Zhou, X. Zhuang, T. Rabczuk. Phase field modeling of brittle compressive-shear fractures in rock-like materials: A new driving force and a hybrid formulation. *Computer Methods in Applied Mechanics and Engineering*, 355: 729–752, 2019. https://doi.org/10.1016/j.cma.2019.06.021
- [8] M. Wang, W. Shen, J. Liu, J. Shao. Phase-field modeling of cracking process in partially saturated porous media and application to rainfall-induced landslides. *Engineering Geology*, 310, 106884, 2022. https://doi.org/10.1016/j.enggeo.2022.106884
- [9] R.J.M. Geelen, Y. Liu, T. Hu, M.R. Tupek, J.E. Dolbow. A phase-field formulation for dynamic cohesive fracture. *Computer Methods in Applied Mechanics and Engineering*, 348: 680–711, 2019. https://doi.org/10.1016/j.cma.2019.01.026
- [10] K.H. Pham, K. Ravi-Chandar, C.M. Landis. Experimental validation of a phase-field model for fracture. *International Journal of Fracture*, 205:83–101, 2017. https://doi.org/10.1007/s10704-017-0185-3
- [11] X. Zhang, S.W. Sloan, C. Vignes, D. Sheng. A modification of the phase-field model for mixed mode crack propagation in rock-like materials. *Computer Methods in Applied Mechanics and Engineering*, 322: 123–136, 2017. https://doi.org/10.1016/j.cma.2017.04.028
- [12] M. Ambati, T. Gerasimov, L. De Lorenzis. A review on phase-field models of brittle fracture and a new fast hybrid formulation. *Computational Mechanics* 55: 383–405, 2015. https://doi.org/10.1007/s00466-014-1109-y
- [13] N. Sukumar, A. Tabarraei. Conforming polygonal finite elements. *International Journal for Numerical Methods in Engineering*, 61:2045–2066, 2004. https://doi.org/10.1002/nme.1141
- [14] S.E. Mousavi, Z. Xiao, N. Sukumar. Generalized Gaussian quadrature rules on arbitrary polygons. *International Journal for Numerical Methods in Engineering*, 82: 82:99–113, 2010. https://doi.org/10.1002/nme.2759
- [15] C. Talischi, G.H. Paulino, A. Pereira, I.F.M Menezes. PolyMesher: a general-purpose mesh generator for polygonal elements written in Matlab. *Structural and Multidisciplinary Optimization*, 45:309–328, 2012. https://doi.org/10.1007/s00158-011-0706-z
- [16] C. Talischi, G.H. Paulino, A. Pereira, I.F.M. Menezes. PolyTop: a Matlab implementation of a general topology optimization framework using unstructured polygonal finite element meshes. *Structural and Multidisciplinary Optimization*, 45:329–357, 2012. https://doi.org/10.1007/s00158-011-0696-x
- [17] E.L. Wachspress. *A Rational Finite Element Basis*. Academic Press: New York, NY, 1975.
- [18] S. Li, X. Cui. N-sided polygonal smoothed finite element method (nSFEM) with non-matching meshes and their applications for brittle fracture problems. *Computer Methods in Applied Mechanics and Engineering*, 359, 112672, 2020. https://doi.org/10.1016/j.cma.2019.112672
- [19] B. Bourdin, G.A. Francfort, J-J. Marigo. Numerical experiments in revisited brittle fracture. *Journal of the Mechanics and Physics of Solids*, 48: 797–826, 2000. https://doi.org/10.1016/S0022-5096(99)00028-9

[20] X. Xiang, D. Zi-Hang. Numerical implementation of a modified Mohr–Coulomb model and its application in slope stability analysis. *Journal of Modern Transportation*, 25: 40–51, 2017. https://doi.org/10.1007/s40534-017-0123-0

Timo Saksala, Reijo Kouhia Structural mechanics, BEN, Tampere University P.O. Box 600, FI-33101 Tampere timo.saksala@tuni.fi, reijo.kouhia@tuni.fi

Mahmood Jabareen Faculty of Civil and Environmental Engineering, Technion-Israel Institute of Technology, Haifa, Israel cvjmah@technion.ac.il

# Appendix A

A mesh sensitivity study is performed here with the pre-notched PMMA specimen, however, removing the sharp crack because the meshing algorithm by Talischi et al. [15] cannot handle such a fine detail successfully. The boundary conditions and the material properties are the same as those used above. However, the length scale parameter is adjusted according to the element size in the meshes shown in Figure 6 so that  $l_c = 2$  mm,  $l_c = 1.5$  mm, and  $l_c = 1$  mm for meshes with 2000, 4000, and 8000 elements, respectively.

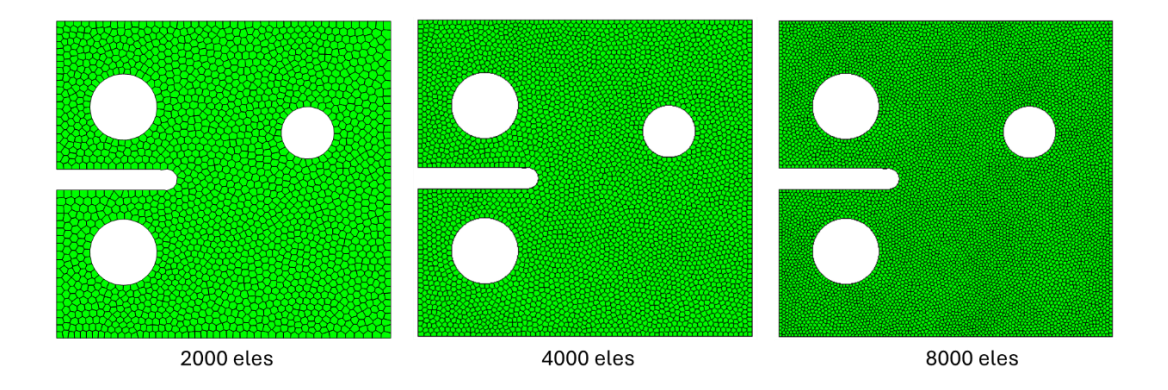


Figure 6. The polygonal meshes with 2000, 4000, and 8000 polygons for the mesh sensitivity study with the pre-notched tension specimen.

The simulation results are shown in Figure 7. The crack path starts at the tip of the notch and propagates to the edge of the extra hole with each mesh, albeit with differing details (Figure 7a). The corresponding force-crack opening displacement (COD) curves in Figure 7b show that the mesh with 2000 elements is too coarse while the two denser meshes result in much more similar force-COD responses. This, together with the crack path details, suggest that the finest mesh here is enough for this problem. In any case, the simulations here show that the present formulation of the phase field method with polygonal elements is mesh sensitive.

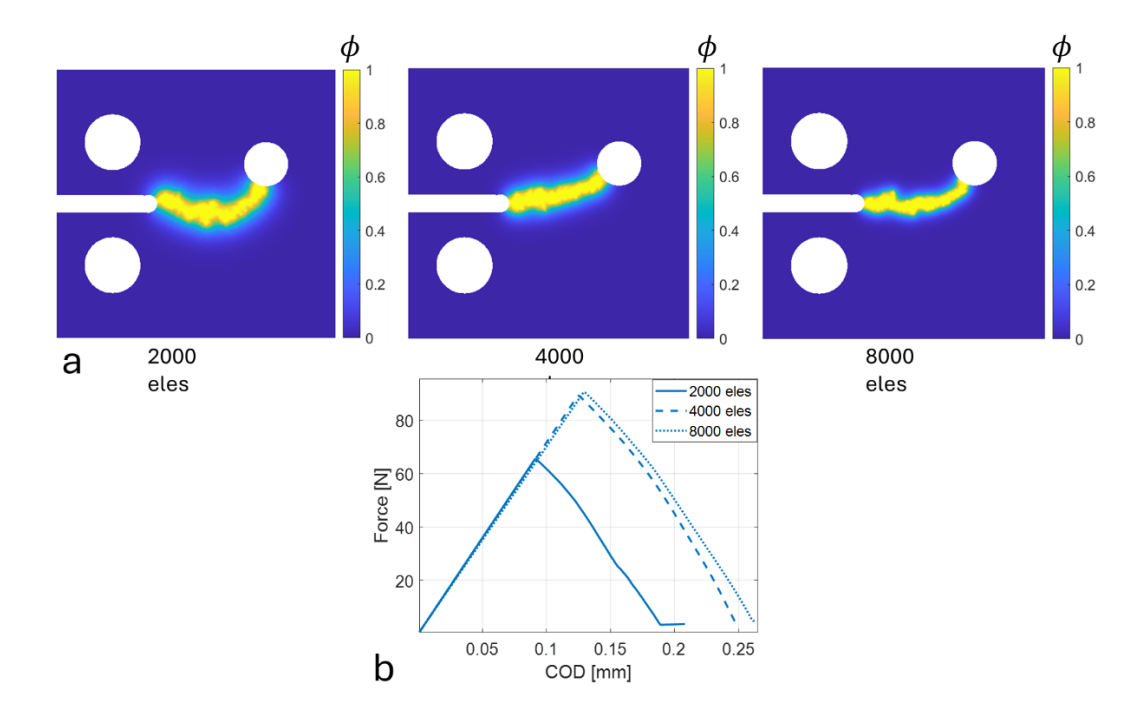


Figure 7. Simulation results for the mesh sensitivity study with the pre-notched tension specimen: The predicted failure modes in terms of the phase field variable (a); The corresponding force-crack opening responses (b).